Supporting Information

Molecular Dynamics Study on Interfacial Heat Transport in Carbon Nanotube/conjugated polymer composites

Xingyu Pan[1], Zhenjie Zhang[1], Xiyue Gao[1], Dongyue Jiang[2],Xiaoliang Zhang[2,*], Lujun Pan[1,*], Zeng Fan[1,*]

[1] School of Physics, Dalian University of Technology, Dalian, Liaoning 116024, China

[2] Key Laboratory of Ocean Energy Utilization and Energy Conservation of Ministry of Education, School of Energy and Power Engineering, Dalian University of Technology, Dalian, Liaoning 116024, China

Corresponding authors. zhangxiaoliang@dlut.edu.cn (X. Zhang), lpan@dlut.edu.cn (L. Pan), fanzeng@dlut.edu.cn (Z. Fan)

S1. Details of Lennard-Jones (LJ) parameters

The Lennard-Jones (LJ) parameters are shown in Table S1. The Lorentz Berthelot combining rule was used in this work for mixed interactions by the following formula:

$$\sigma = \frac{\sigma_1 + \sigma_2}{2} \tag{1}$$

$$\varepsilon = \sqrt{\varepsilon_1 \cdot \varepsilon_2} \tag{2}$$

Table S1 Details of LJ parameters.

Atoms	**ε/eV**	**σ/Å**
C-H	0.0043	1.00
C-C	0.0046	3.85
C-O	0.0065	3.69
C-S	0.0082	3.94
C-Cl^-	0.0067	3.89

S2. Comparison of interface thermal conductivity under different heat fluxes

As shown in Table S2, the results indicated that under different heat flux, the standard deviation exhibited by G_L was only 5.35×10^{-4}. This verified that under this calculation condition, the result has no direct connection with the selection of heat flow. Therefore, the heat flux calculation in this work, a constant of 0.3 $eVps^{-1}$ was used as the heat flux to construct the temperature difference.

Table S2 Details of interface thermal conductivity with different heat flux

Heat flux/$eVps^{-1}$	**G_L/ $Wm^{-1}K^{-1}$**
0.1	0.0290
0.2	0.0301
0.25	0.0305
0.3	0.0316
0.35	0.0309
0.4	0.0307

S3. The temperature evolves over the simulation time

As shown in Figure S1, after a simulation of 1.6 ns, the temperature difference no longer changed. To further illustrate the sufficiency of the simulation time, we also extended the simulation time form 3.0 ns to 4 ns. The results showed that as the time lengthened, the temperature difference did not undergo significant changes. Under the condition of saving the simulation time, choosing a simulation time of 1.6 ns was already sufficient.

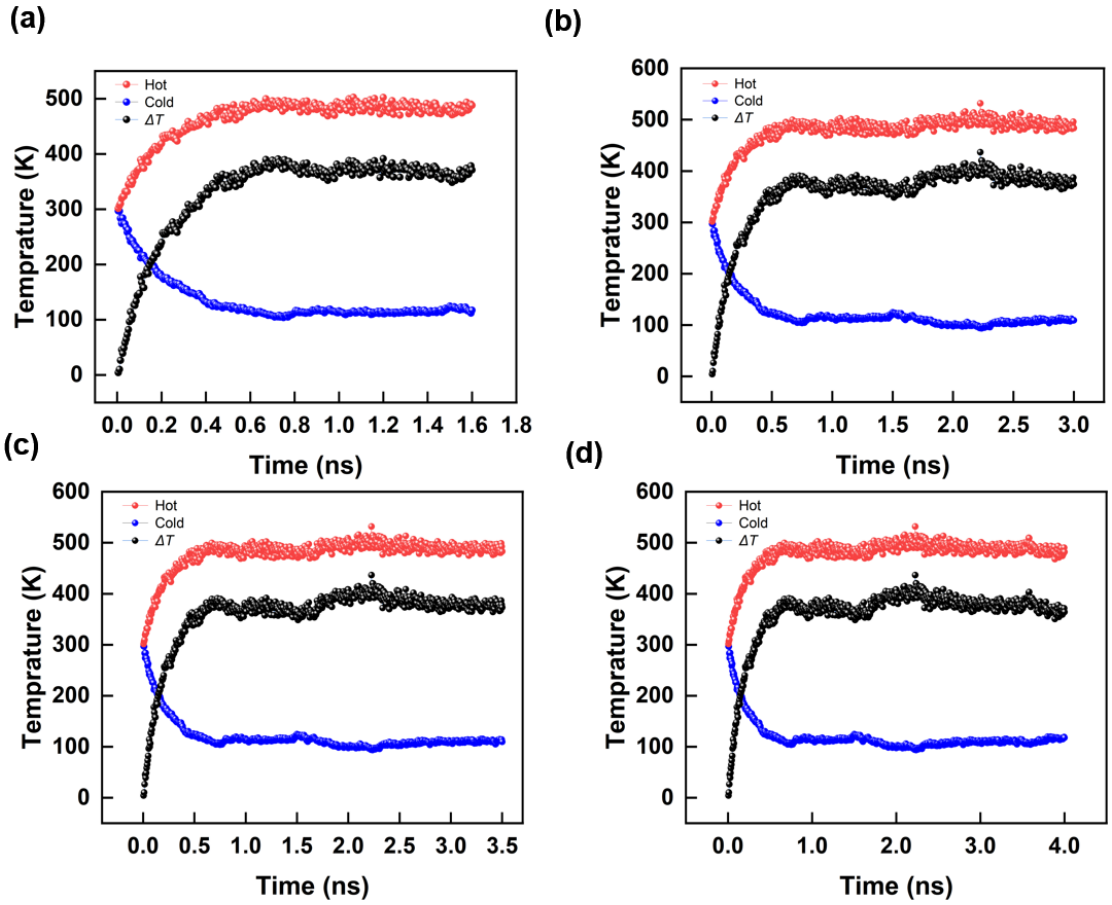

Figure S1. The temperature of (6,6) SWNT over extended simulation time. (a) 1.6 ns (b) 3.0 ns, (c) 3.5 ns and (d) 4.0 ns.

S4. The temperature profiles

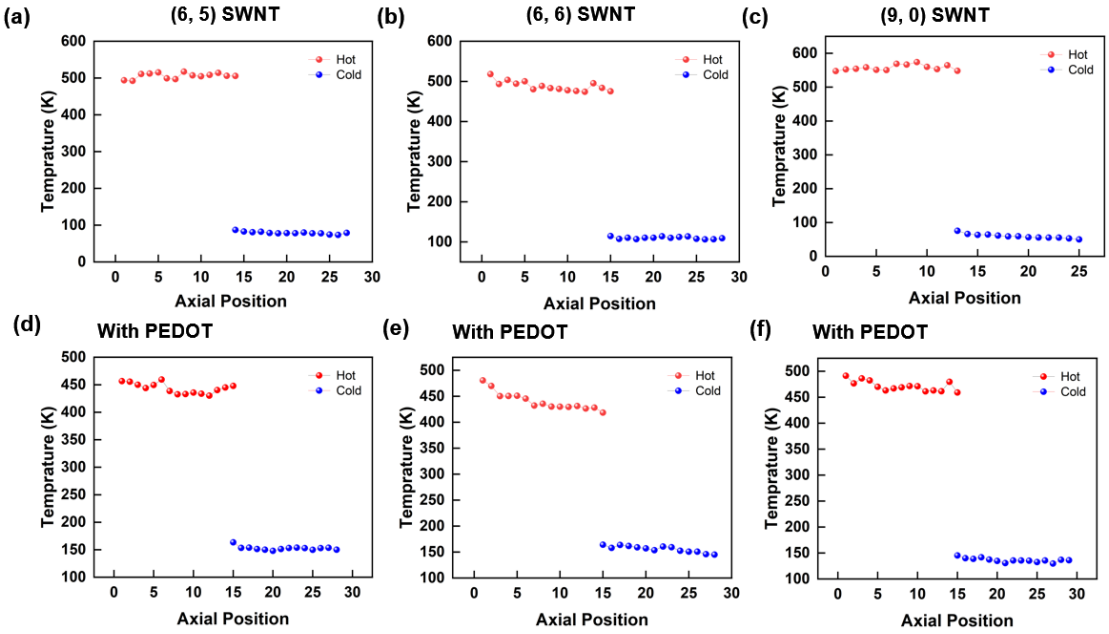

FigureS2. The temperature profile of (a) (6,5) SWNT, (b) (6,6) SWNT, (c) (9,0) SWNT, (d) (6,5) SWNT with PEDOT, (e) (6,6) SWNT with PEDOT, (f) (9,0) SWNT with PEDOT.

S5. Comparison of the temperatures of near-interface region and overlap region

Since the definition of the interface of such systems is not yet fully clear, in this work we approximate the atoms in the overlap region as interfacial atoms and represent the average temperature difference of the atoms in this region as the temperature difference between the two SWNTs. This method is often adopted in calculating ΔT in interface issues [1-3]. We also conducted relevant calculations on the temperatures of the atoms in the near-interface region. The results showed that ΔT between the atoms in the overlap region and the near-interface region is almost the same. The relevant calculation results are provided in Table S3.

Table S3 Comparison of temperatures in Overlap region and Near-interface region

Chirality	Temperature			
	Region	$T_{SWNT\ hot}$ /K	$T_{SWNT\ cold}$/K	ΔT/K
(6,5) SWNT	Near-interface region	482	76	406
	Overlap region	504	81	423

(6,6) SWNT	Near-interface region	458	200	358
	Overlap region	481	119	362
(9,0) SWNT	Near-interface region	544	63	481
	Overlap region	558	65	493

S6. G_L for SWNTs of various chiralities under distinct random number conditions

We also validated the G_L results of neat SWNT systems by adjusting the random number seeds. As shown in Table S4, results indicate that under different random heat flux conditions, G_L shows almost no change with the variation of random number seeds. The maximum standard deviation is only 0.002 W m^{-1} K^{-1}, indicating the stability of the data.

Table S4 G_L for SWNTs of various chiralities under distinct random number conditions

SWNT chirality	G_L /W m^{-1} K^{-1}		$G_{L,\,avg}$ /W m^{-1} K^{-1}	Standard deviation /W m^{-1} K^{-1}
(6,5)	Run 1	0.0284	0.02825	2.13×10^{-4}
	Run 2	0.0283		
	Run 3	0.0280		
(6,6)	Run 1	0.0332	0.03093	2.00×10^{-3}
	Run 2	0.0290		
	Run 3	0.0307		
(9,0)	Run 1	0.0244	0.02394	7.58×10^{-4}
	Run 2	0.0243		
	Run 3	0.0231		

S7. The effect of SWNT length on the G_L

We chose (6,6) SWNT as research object and calculated G_L as a function of its length. As shown in Figure S3, the results show that the interface thermal conductivity is affected by the size effect. When the length is too small, G_L is abnormally high. This might be related to the fact that the interface position is too close to the heat source. As the size gradually increases, the size effect begins to weaken and eventually stabilizes at around 0.030 $Wm^{-1}K^{-1}$.

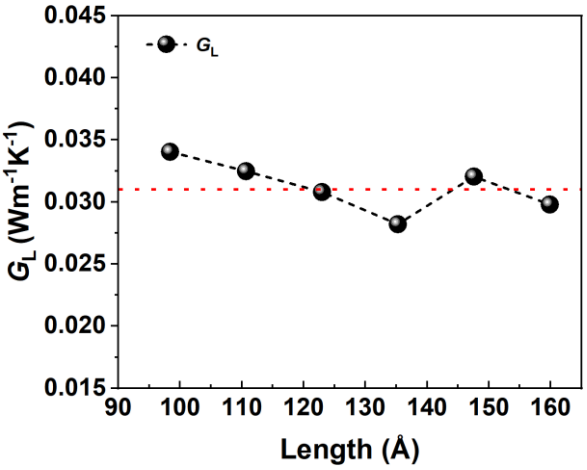

Figure S3. G_L as a function of (6,6) SWNT length

S8. Vibrational density of states (VDOS) of SWNTs in neat SWNT systems

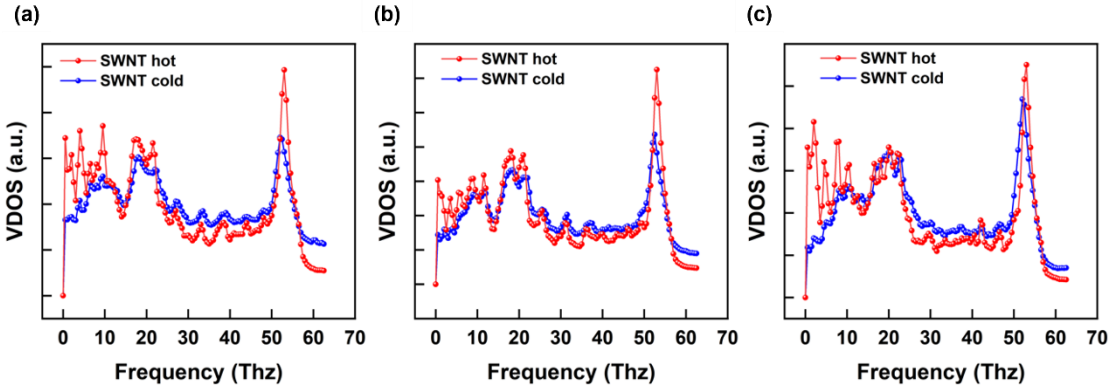

Figure S4. Vibrational density of states (VDOS) of hot- and cold-end SWNTs in neat SWNT systems. Systems composed of (a) (6,5), (b) (6,6) and (c) (9, 0) SWNTs.

S9. Interatomic interaction energy

Table S5 Details of interatomic interaction energy.

Atoms	Energy/eV
C-H	-0.0065231
C-C (main chain)	-7.49905
C-C (side chain)	-3.29007
C-S	-4.62566
C-O	-3.78506

S10. The temperature stability of PEDOT chains

To verify the stability of data, as shown in Figure S5, the temperature of the entire PEDOT chain (average temperature) in (6,6) SWNT with n=12 PEODT

system did not change with prolonged simulation time, and no chemical bond breaks or other degradation phenomena occurred in PEDOTs at this temperature difference condition.

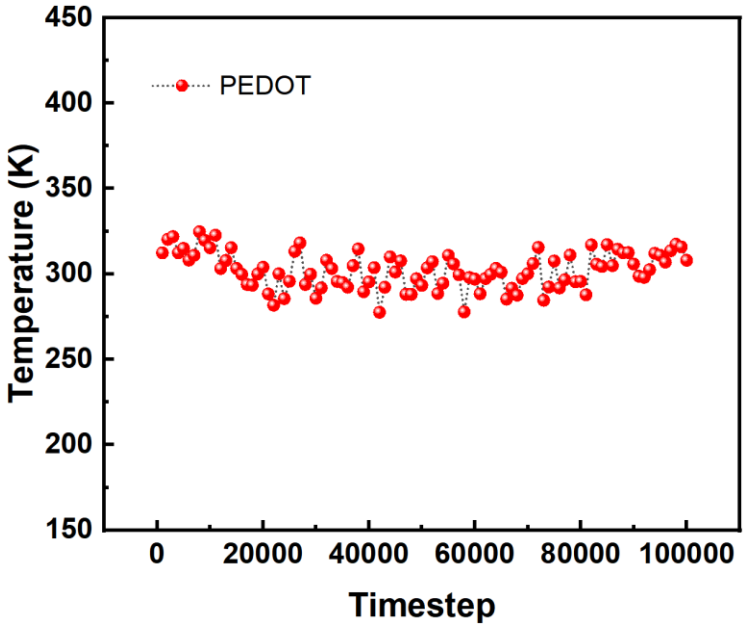

Figure S5. Temperature evolution of PEDOT chains over extended simulation time.

S11. The method for calculating the heat flow distribution ----Fivi method

In order to study the proportion of heat flux distributed to the SWNT-SWNT channel and the SWNT-polymer-SWNT channel, the Fivi method was employed. In this method the heat flux was evaluated by:

$$J^{\beta}_{\mathrm{A}\to\mathrm{B}} = -\frac{1}{2S}\sum_{\alpha}\sum_{i\in\mathrm{A}}\sum_{j\in\mathrm{B}} F^{\beta}_{ij\alpha}\left(\upsilon_{i\alpha}+\upsilon_{j\alpha}\right) \tag{3}$$

where β denotes a force such as stretching, bending, proper, improper, LJ, or Coulombic component. α is x, y, or z direction; S is the cross-section area between A and B; Fijα is the force acting on atom i by atom j in the α direction; and υiα is the velocity of atom i in the α direction.

The distribution of the two channels of different chiral SWNTs after the addition

of polymers is shown in the Figure S6.

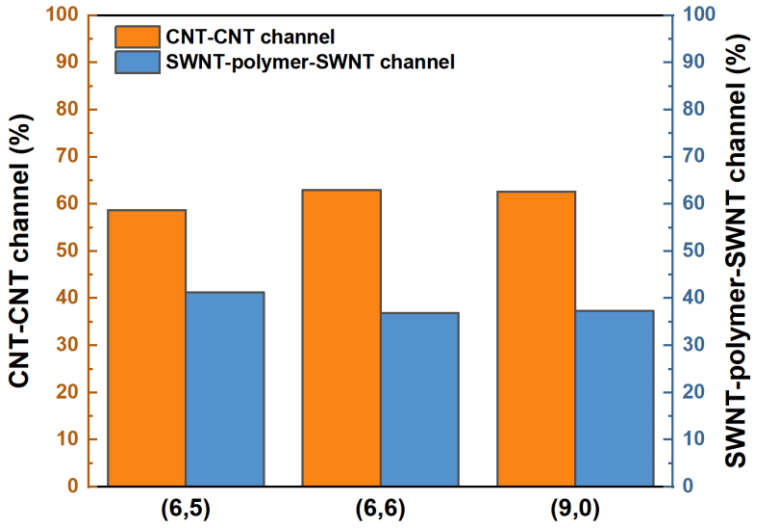

Figure S6. The distribution of the two channels of different chiral SWNTs after the addition of polymers.

S12. Calculation details of ΔG_L

The ΔG_{L1}, ΔG_{L2} and ΔG_{L3} were calculated through the following method (Taking (6, 5) SWNT as an example):

① Without PEDOT covering, the total conductance is $G_{L,\text{ neat SWNT system}}$ = 0.02841 W m^{-1} K^{-1}.

② When two n = 6 PEDOT chains were added, the total conductance is $G_{L,\text{ SWNT/ PEDOT }(n=6)\text{ composite system}}$ = 0.03851 W m^{-1} K^{-1}.

③ Given that there are totally two PEDOT chains added, if the average contribution from each PEDOT chain was considered, ΔG_{L1} could be calculated by:

$\Delta G_{L1} = 1/2 \times (G_{L,\text{ SWNT/ PEDOT }(n=6)\text{ composite system}} - G_{L,\text{ neat SWNT system}})$ = 0.00505 W m^{-1} K^{-1}.

④ When two n = 12 PEDOT chains were added, the total conductance is $G_{L,\text{ SWNT/ PEDOT }(n=12)\text{ composite system}}$ = 0.04246 W m^{-1} K^{-1}.

In this case, $\Delta G_{L2} = 1/2 \times (G_{L,\text{ SWNT/ PEDOT }(n=12)\text{ composite system}} - G_{L,\text{ SWNT/ PEDOT }(n=6)\text{ composite system}})$ = 0.001975 W m^{-1} K^{-1}.

⑤ When two n = 18 PEDOT chains were added, the total conductance is $G_{L,\text{ SWNT/ PEDOT }(n=18)\text{ composite system}}$ = 0.04986 W m^{-1} K^{-1}.

In this case, $\Delta G_{L3} = 1/2 \times (G_{L,\text{ SWNT/ PEDOT }(n=18)\text{ composite system}} - G_{L,\text{ SWNT/ PEDOT }(n=12)\text{ composite system}})$ = 0.003700 W m^{-1} K^{-1}.

S13. Details of as-calculated $<R_g^2>$

Table S6 $<R_g^2>$ of different PEDOT chains in the SWNT systems with different chirality.

SWNT Chirality / PEDOT chain length	(6, 5)		(6, 6)		(9, 0)	
	Neutral	Doped	Neutral	Doped	Neutral	Doped
6	33.3	26.0	35.2	26.7	32.6	24.8
12	134.5	39.1	171.4	39.4	149.2	40.2
18	122.6	51.3	171.5	49.4	195.4	50.8

S14. Details of density functional theory (DFT) calculations

In Materials Studio 2019, Dmol3 module was used to calculate the energy of Highest Occupied Molecular Orbital (HOMO) and Lowest Unoccupied Molecular Orbital (LUMO) of neutral PEDOT, doped PEDOT and SWNT. Considering the periodic boundary conditions of SWNT, symmetry condition was used in the calculation of SWNT. The PBE functional method was selected, and the Tkatchchenko-Scheffler weak interaction correction was adopted simultaneously. The cut-off energy was set to 400 eV, the maximum number of SCF cycles was set to 500 times, the K-point precision was set to Medium, and the pseudopotentials were OTFG ultra-soft pseudopotentials. The theory of relativity was modified to the Koelling-Harmon method.

S15. Comparison of $\Delta G_L/G_L$ in composite systems with neutral and doped PEDOTs

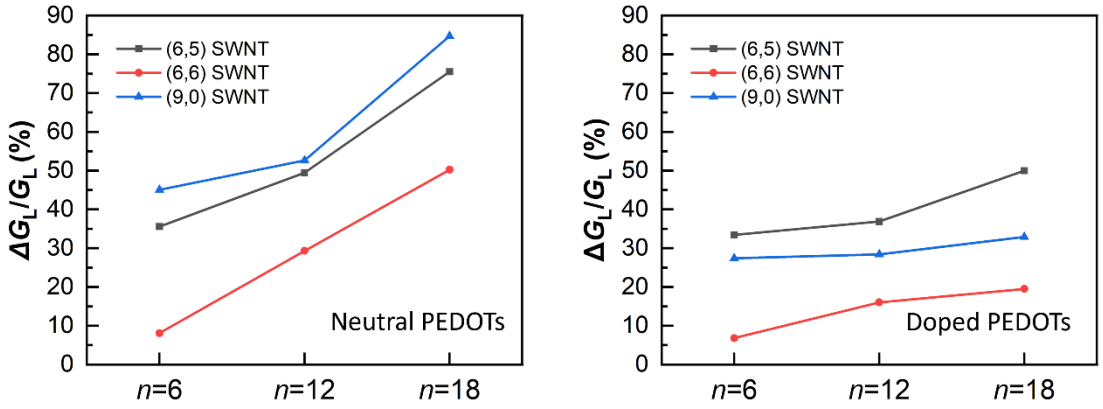

Figure S7. $\Delta G_L/G_L$ in composite systems with different chiral SWNTs as a function of PEDOT chain length. PEDOT chains are in (a) neutral state and (b) doped state, respectively.

S16. Interface interaction energy

As shown in Figure S8(a), the (6,6) SWNT exhibited the strongest interaction energy, followed by (6,5) SWNT, and the (9,0) SWNT had the weakest one. The SWNT with the strongest symmetry has the highest interaction energy, which results in this chiral SWNT having the highest G_L. This further illustrates our proposed viewpoint that the high degree of symmetry is the key factor leading to high G_L. Furthermore, upon the addition of PEDOTs, due to the interaction between PEDOT chains and SWNTs, the interaction energy of these three chiral SWNTs decreases. Among these composite systems, (6,6) SWNT showed the greatest decrease, which can be attributed to the disruption of the symmetry of (6,6) SWNT. It is worth noting that, at this point, the interfacial interaction energy between two SWNTs within the three composite systems are almost identical. This indicates that, from the perspective of interfacial interaction energy, the magnitude of the interaction between SWNT and PEDOT is the main factor influencing G_L. As shown in Figure R6(b), the interfacial interaction energy of (6,5) SWNT with PEDOT is relatively high, while the interfacial interaction energies of (6,6) SWNT and (9,0) SWNT with PEDOT are almost the same. This does not follow the proportional increase rule of G_L observed in these three composite systems. In contrast, the variation in the VDOS within the

low-frequency range shows a significant positive correlation with the proportional increase of G_L. This indicates that, for these composite systems, the addition of PEDOT can effectively enhance interfacial thermal conduction. However, the key factor determining the extent of this enhancement remains the matching degree of the VDOS.

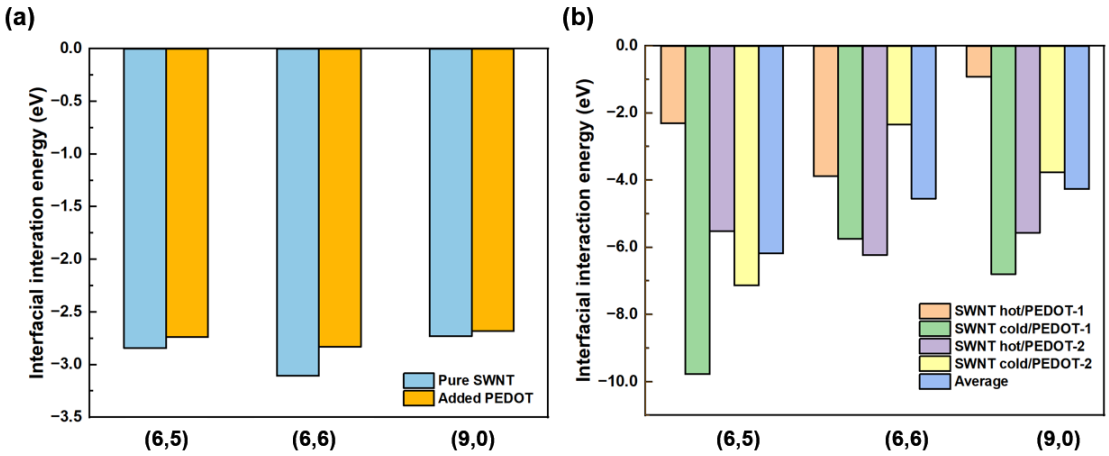

Figure S8. Interfacial interaction energy (a) between hot and cold SWNTs and (b) between an individual SWNT (*i.e.* represented by SWNT hot or SWNT cold) and a PEDOT chain (*i.e.* represented by PEDOT-1 or PEDOT-2) in the composite systems.

S17. Comparison of the overlap integral in the near-interface region and the overlap region

Table S7 comparison of the overlap integral in the near-interface region and the overlap region.

Chirality	**Overlap integral**			
	Region	Neat SWNT	With PEDOT	Grow rate/%
(6,5) SWNT	Near-interface region	0.91	0.95	4.0
	Overlap region	0.89	0.96	7.9
(6,6) SWNT	Near-interface region	0.92	0.93	1.6
	Overlap region	0.90	0.92	2.2
(9,0) SWNT	Near-interface region	0.88	0.95	7.6
	Overlap region	0.88	0.93	5.7

S18. Quantum correction

Since the classical molecular dynamics is not valid for the system temperature below the Debye temperature, quantum corrections must be applied to the temperature and the thermal conductivity predicted by the MD simulations. We considered the quantum effect in the reported NEMD results according to the following expression[4]

$$T_{\mathrm{MD}} = \frac{1}{k_B}\int_0^{\nu_{\max}} D(\nu)\left[\frac{1}{\exp\left(h\nu/k_B T_{qc}\right)-1}+\frac{1}{2}\right]h\nu \,\mathrm{d}\nu \qquad (4)$$

where ν is phonon frequency,$D(\nu)$ is the normalized vibrational density of states (VDOS) of SWNT calculated by taking the Fourier transform of the atomic velocity autocorrelation function (VACF) from the MD simulation $\nu_{\max}$ is the maximal phonon frequency of VDOS,1/[exp($h\nu/kBTqc$) − 1] is the Bose-Einstein distribution and h is the Planck constant, $d\nu$ is the minimum frequency interval of VDOS; and T_{MD} and Tqc are the MD and quantum-corrected temperature, respectively.

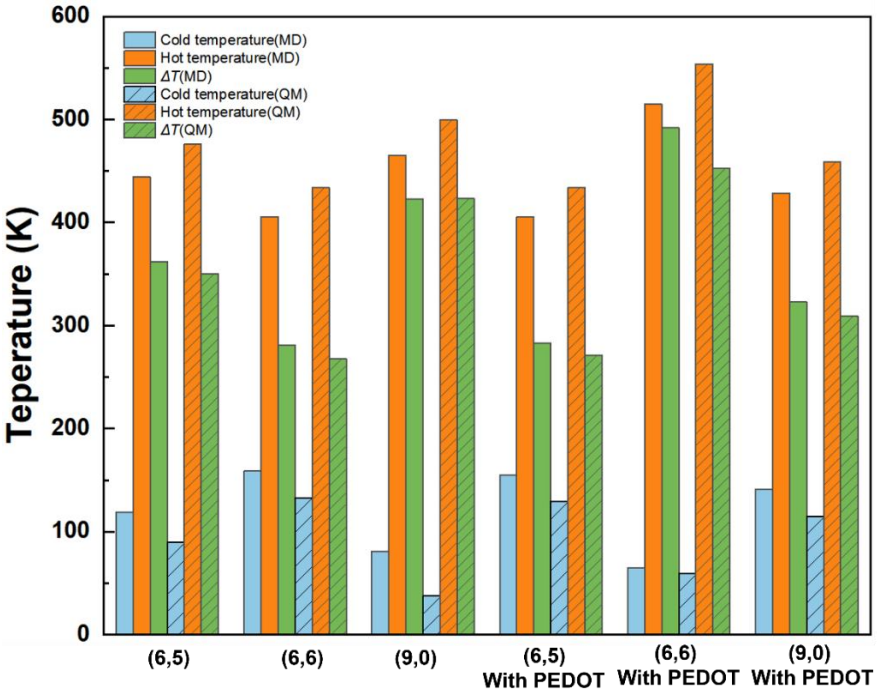

Figure S9. Comparison of temperature quantum correction results of SWNTs with different chiralities and SWNTs with different chiralities after the addition of PEDOT

Reference

1. Y. Xu, L. Yang and Y. Zhou, Physical Chemistry Chemical Physics, 2022, 24, 24503-24513.
2. Y. Xu, B.-Y. Cao and Y. Zhou, International Journal of Heat and Mass Transfer, 2024, 232, 125943.
3. H. Zou, Y. Feng, X. Tang, X. Zhang and L. Qiu, Composites Science and Technology, 2024, 245, 110346.
4. C. Z. Wang, C. T. Chan and K. M. Ho, Physical Review B, 1990, 42, 11276-11283.